UAV-Relay-Assisted Live Layered Video Multicast for Cell-Edge Users in NOMA Networks

Hang Shen, *Member, IEEE*, Ziyuan Tong, Tianjing Wang, *Member, IEEE*, and Guangwei Bai

Abstract—In this paper, a live layered video multicast framework based on unmanned aerial vehicle (UAV) relays is presented for on-orthogonal multiple access (NOMA) networks, aiming to maximize the aggregated video reception quality for cell-edge users. A visualizable graph model is constructed to characterize the coupling of the deployment of UAVs and their association with multicast groups with interference cancellation. Based on this graph model, the problem of maximizing multicast group video reception quality is modeled as a clique-based nonlinear integer programming and decoupled into UAV placement and UAV-group association subproblem and subchannel allocation subproblem. For mathematical traceability, the former is transformed into a unique maximum weight clique problem under the available UAV number constraint, solved by an improved branch-and-bound algorithm. For the latter, a heuristic resource-matching strategy is designed to obtain a near-optimal subchannel allocation with low computational complexity. Simulation results demonstrate that the proposed scheme outperforms mainstream benchmarks in terms of aggregate peak signal-to-noise ratio (PSNR), spectrum utilization, network coverage, and adaptability.

Index Terms—UAV, NOMA, layered video multicast, resource allocation.

I. Introduction

WITH the advancement of networking technologies, real-time video services (e.g., live sports streaming, concert venues) have become ubiquitous in people's daily lives. In its report "Network Traffic Forecast: 2019-2024",[1] Omdia states that video is expected to account for over 75% of total wireless network traffic by 2025. The surge of real-time video traffic has imposed tremendous pressure on network resource allocation. Compared to unicasting, multicasting can provide services to multiple users with bandwidth independent of the number of users [1]. By leveraging multicasting for real-time video, substantial savings in the base station (BS) bandwidth can be achieved [2]. These efficiencies make multicasting well-suited for supporting the rising demands of bandwidth-intensive, real-time live video services.

Scalable video coding (SVC) [3] encodes a video stream into multiple layers of resolution, quality, and frame rate, by which devices can adjust the number of decoded layers according to network conditions and decoding capabilities, reconstructing the complete video. Due to flexibility and adaptivity, SVC has become a promising video multicasting technique. Using orthogonal multiple access (OMA), each video layer is transmitted over different orthogonal channels. Via power domain multiplexing, non-orthogonal multiple access (NOMA) can serve multiple users in the same channel [4], [5]. When receiving different video layers non-orthogonal, an end device can run successive interference cancellation (SIC) [6] to demodulate signals according to the received power strength.

The link between BS-edge users and the BS is usually a non-line-of-sight (NLoS) connection [7]. Relying solely on terrestrial BSs may not guarantee high-quality video reception for BS-edge users. UAVs' flexible deployment, low transmit power, and lightweight nature make them well-suited to provide BS-edge video multicast/broadcast services. Their ability to fly at optimal altitudes and establish line-of-sight (LoS) links help expand BS coverage and reduce resource consumption for data distribution [8]. With NOMA, UAVs deployed at BS-edge can share spectrum with the BS and superimpose signals of different video layers in the power domain, improving multicast service quality and resource utilization. Although UAVs have limited energy and communication capabilities, their continued improvement and intelligent deployment can enable high-quality video multicasting services for the challenging NLoS conditions typical of BS coverage edge.

A. Challenging Issues and Related Works

For UAV-relay-enhanced online SVC video multicasting for BS-edge in NOMA networks, many challenges remain:

1) UAV-BS Cooperation: Most existing hierarchical video multicast schemes target terrestrial cellular networks. In [9], the adaptive mobile streaming transmission was formulated as a multi-source multicast multi-rate problem, decomposed in terms of clients, and solved by a distributed delivery algorithm. Zhu et al. explored a NOMA-enabled SVC multicast scheme with ground BSs sending base and enhancement layers [10]. Improving from this scheme, Dani et al. propose a joint power allocation and subgrouping scheme to maximize the sum multicast rate under maximum transmit power and proportional rate constraints [11]. Many UAV-aided video

[1]Omdia. (2020) https://omdia.tech.informa.com/OM011420/Radio-Access-Network-Forecast-201924.

distribution schemes are cache-enabled, where UAVs provide offline services to users [12], [13], [14], and the video cache must be updated regularly to improve the hit rate [15]. For supporting real-time video, one approach is to establish backhaul links to the BS via millimeter wave (mmWave) [16]. However, due to the high propagation loss of signals, mmWave has a limited communication range [17], less than the coverage radius of a macro BS, making it difficult for UAVs placed at BS-edge to maintain stable backhaul connections. Li et al. [18] develop a random network coding scheme for UAV multicast networks, incorporating a sliding coding window scheduling for encoding and a lower triangular coding structure for decoding. Comşa et al. [19] design a learning-based scheduling solution deployed in UAV-based networks to support immersive live omnidirectional virtual reality video streaming. However, those works did not consider the interaction between UAVs and the BS. In [20], a position-based beamforming algorithm is presented to improve the backhaul transmission of 5G UAV broadcasting by tracking mobility and steering the antenna beam to target the UAVs. Although UAV-BS interaction is considered, the potential gain obtained in combination with NOMA needs further investigation.

2) Decoding of Layered Videos With Multi-UAVs: A common hierarchical video multicast strategy is the macro BS sending base layer and multiple small-cell sending enhancement layers [21]. Compared to enhancement layers, the base layer requires a higher transmission rate, meaning more bandwidth resources are consumed at the macro BS. UAVs can deliver base layers using LoS links with less resource consumption. After receiving video layers, NOMA devices decode and cancel interference according to the power strength order. Note that for SVC NOMA multicast, the video reception must consider both video layer dependencies and reception order, in which the video layer reception order becomes one constraint for UAV deployment, which still needs to be studied. Katwe et al. investigate multi-UAV cooperative full-duplex NOMA systems by clustering users, placing UAVs, and allocating power to improve throughput [22]. Based on fountain-coded coordinated multipoint, a 5G multimedia service framework based on UAV full-duplex relay is developed for high-reliability, low-latency broadcast communication [23]. Zeng et al. propose joint power allocation and UAV trajectory design to enhance user reception rate [24]. In [25], a resource allocation framework is presented for UAV-assisted multicast wireless networks. The power allocation and UAV trajectory design were formulated as non-linear and non-convex optimization problems for offline and online scenarios. However, these methods cannot accommodate layered video delivery.

3) UAV-Group Association Patterns: Associating each multicast group with a unique UAV can avoid co-channel interference but fails to exploit UAVs' flexibility. Allowing one multicast group to associate with multiple UAVs increases service flexibility, but the superimposed UAV signals may negate the spectral reuse gains. Most existing works consider an unicast service scenario. Zeng et al. study layered caching at multiple UAVs to minimize access latency through joint cache placement, UAV deployment, and user association [15].

Wang et al. design a multi-agent Q-learning algorithm for uplink transmission in UAV-assisted cellular networks to determine UAV deployment and association with minimum energy consumption of users and UAVs [26]. Li et al. aim to maximize the network energy efficiency by jointly optimizing the UAV-user association, UAV position, and resource allocation [27]. An energy-constrained coalition game was proposed to solve the UAV user association problem. These research works did not consider layered video multicasting.

B. Contributions and Organization

Considering a scenario where multiple UAVs serve as relays to provide online video multicast services to BS-edge users, we present a BS-UAV cooperative NOMA framework for SVC video multicasting to maximize multicast groups' aggregated video reception quality in BS-edge areas. The main contributions are three folded:

- A visualizable graph model is constructed to characterize the coupling between decision variables (for UAV deployment and multicast group association) and video decoding (for sequential superposition and SIC). Each clique in the graph corresponds to a set of decisions meeting the requirements on superposition coding and SIC.
- Based on the proposed graph model, the multicast video quality maximization problem is transformed into a clique-based nonlinear integer programming. Due to the high computational complexity, the problem is decoupled into UAV-group association and subchannel allocation subproblems to facilitate processing.
- The former subproblem is converted into a particular maximum weight clique problem, and an improved branch-and-bound algorithm is developed to determine the UAV placement and UAV-group association. A low-complexity heuristic matching strategy is designed to obtain a near-optimal resource allocation scheme for the latter. Extensive simulation results demonstrate that the proposed scheme outperforms benchmark approaches in aggregated peak signal-to-noise ratio (PSNR), spectrum efficiency, and BS-edge coverage.

The remainder of this paper is organized as follows. Section II presents the communication and UAV deployment models and the video reception and decoding framework. In Section III, the video quality maximization problem for BS-edge is modeled as a clique-based program. Section IV decouples the optimization problem and presents the solutions. Section V designs simulation experiments for performance evaluation. Section VI summarizes the study and discusses follow-up works. The main symbols used are listed in Table I.

II. SYSTEM MODEL

In the scenario shown in Fig. 1, multiple UAVs are deployed at the edge of the BS and serve as relays. There are three types of links: the BS-to-UAV link (B2U), the BS-to-device link (B2D), and the UAV-to-device link (U2D). Users requesting the same video stream belong to one multicast group. A multicast group can be associated with one or more UAVs, i.e., multiple UAVs can serve one multicast group. In the scenario,

TABLE I
MAIN NOTATIONS AND VARIABLES

Symbol	Definition
b_n	Num. of subchannels allocated to group n
B	Total num. of subchannels
$\mathcal{C}/C$	Set/Num. of vertices of a clique
e	Bandwidth of each subchannel
$h_{i,j}$	Horizontal distance between $l_{j,k}$ and user i
$h_{i,m}$	Horizontal distance between the BS and user i
$\mathcal{I}_n$	Set/Num. of devices in multicast group n
$\mathcal{I}_{j,k,n}$	Set/Num. of devices covered by a UAV at $l_{j,k}$ in multicast group n
$\mathcal{J}$	Set of UAV projection positions in x-y plane
$\mathcal{K}_j$	Set of candidate UAV flight heights on (x_j, y_j)
$l_{j,k}$	UAV 3D placement coordinate $(x_j, y_j, z_{j,k})$
$\mathcal{N}/N$	Set/Num. of multicast groups
p_u/p_m	UAV/BS transmit power
$q_{j,k,n}$	0-1 variable indicating association between a UAV at $l_{j,k}$ and group n
$\text{PSNR}_{1,n}$	PSNR of receiving the base layer for group n
$\text{PSNR}_{2,n}$	PSNR of receiving base and enhancement layers for multicast group n
$R_{j,k}$	Coverage radius of a UAV at $l_{j,k}$
$u_{1,n,i}/u_{2,n,i}$	0-1 variable indicating device i receiving base layer/enhancement layer
α	Num. of available UAVs
$\eta_{\text{LoS}}/\eta_{\text{NLoS}}$	Additional path loss of the D2U LoS/NLoS link
$\lambda_{1,n}/\lambda_{2,n}$	Minimum bitrate for group n to decode the base layer and the enhancement layer
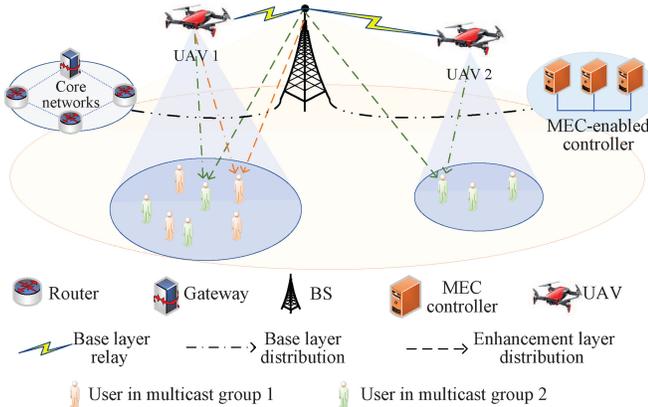
Fig. 1. UAV-relayed online SVC multicast scenario.

multicast group 1 is associated with UAV 2, and multicast group 2 is associated with UAVs 1 and 2. By accessing global information, the MEC-enabled controller determines UAVs' placement and association patterns with multicast groups and allocates resources to each group.

Each video is encoded using SVC into a base and enhancement layers. Different orthogonal subchannels are allocated to each multicast group. For instance, multicast groups 1 and 2 in Fig. 1 are allocated 4 and 5 subchannels, corresponding to the shaded and unshaded parts in Fig. 2. The former represents BS's spectrum resources for sending the base layer to UAVs over B2U links. The latter represents the spectrum resources shared by U2D links (UAVs sending base layers to users through U2D links) and B2D links (BS sending enhancement layers to users).
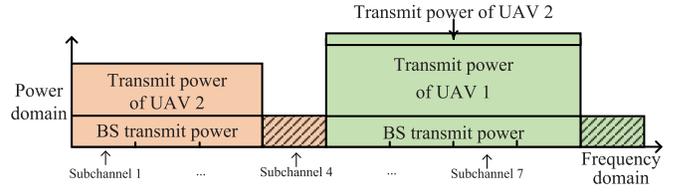
Fig. 2. Superposition in power domain and spectrum partition.

A. Communication Model

Let $l_{j,k} = (x_j, y_j, z_{j,k})$ denote a candidate UAV 3D deployment position, where $j \in \mathcal{J}$ is the index of projection position in the x-y plane, $k \in \mathcal{K}_j$ is the height index on (x_j, y_j), and $\mathcal{J}$ and $\mathcal{K}_j$ are the index sets. The LoS communication probability between a UAV at $l_{j,k}$ and ground device i is defined as [28]

$$P_{\text{LoS}}(h_{i,j}, z_{j,k}) = \frac{1}{1 + a\exp\left(-o(\arctan(\frac{z_{j,k}}{h_{i,j}}) - a)\right)} \quad (1)$$

where $h_{i,j}$ is the horizontal distance between the UAV and device i. a and o are environment-related parameters. The path loss model from the UAV to the device is calculated as [29]

$$\phi(h_{i,j}, z_{j,k}) = 20\log\left(\frac{4\pi c\sqrt{h_{i,j}^2 + z_{j,k}^2}}{s}\right) + P_{\text{LoS}}(h_{i,j}, z_{j,k})\eta_{\text{LoS}} + (1 - P_{\text{LoS}}(h_{i,j}, z_{j,k}))\eta_{\text{NLoS}} \quad (2)$$

where c is the carrier frequency, s is the speed of light. η_{LoS} and η_{NLoS} represent the additional path loss over the D2U LoS and NLoS links, respectively.

The azimuth and elevation angles of the directional antenna equipped on the UAV are denoted as θ_1 and θ_2, respectively. Assume the antenna's half-power beamwidth is the same for both azimuth and elevation. The antenna gain in azimuth angle (θ_1, θ_2) is given by [30]

$$f(\theta) = \begin{cases} \frac{f_1}{\theta^2}, & \text{if } 0 \leq \theta_1 \leq \theta, 0 \leq \theta_2 \leq \theta \\ f_0 \approx 0, & \text{otherwise} \end{cases} \quad (3)$$

where $f_1 = \frac{30000}{2^2} \times (\frac{\pi}{180})^2 \approx 2.2846$ and f_0 denotes the antenna gain outside the 3dB beamwidth. Since $0 < f_0 \ll \frac{f_1}{\theta^2}$ in practice, the antenna gain is simplified as $f_0 = 0$ [31].

Based on (2) and (3), the channel gain from a UAV at $l_{j,k}$ to its covered device i is denoted as $g_{j,k,i} = 10^{-\frac{f(\theta)\phi(z_{j,k}, h_{i,j})}{10}}$. Let (x_m, y_m, z_m) denote BS coordinates. The channel gain from the BS to ground device i is calculated as $g_{i,m} = 30 + 35\log(h_{i,m})$ using the method described by Ye et al. [32], where $h_{i,m} = \sqrt{(x_m - x_i)^2 + (y_m - y_i)^2}$ is the horizontal distance between the BS and device i. For a UAV at $l_{j,k}$, its effective coverage radius relies on LoS probability and free space path-loss, calculated as [33]

$$R_{j,k} = \min\left\{\frac{z_{j,k}}{\tan\left(a - \frac{1}{o}\ln\frac{1-\xi}{a\xi}\right)}, \sqrt{\left(\frac{s10^{\frac{\psi}{20}}}{4\pi c}\right)^2 - z_{j,k}^2}\right\} \quad (4)$$

denoting the minimum of the two expressions for $z_{j,k}$, where ξ is the LoS probability and ψ represents the free space path-loss threshold. The first and second terms contained in the
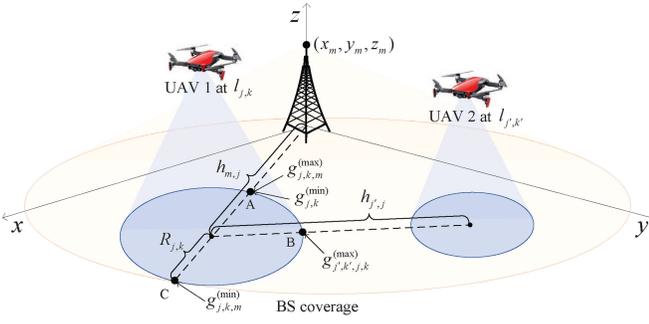
Fig. 3.   Impact of UAV deployment on SIC.

min{} in (4) increase and decrease monotonically with $z_{j,k}$, respectively. When $z_{j,k}$ is small (large), the first term is less (larger) than the second term. Accordingly, the effective coverage radius of a DSC at $l_{j,k}$ increases first and decreases as its flight altitude, $z_{j,k}$, increases.

B. UAV Deployment Model

Ground devices perform interference cancellation according to the received signal strength. In Fig. 1, multicast group 1 is associated with UAVs 1 and 2. When receiving signals from UAV 1 and the BS, devices under the coverage of UAV 1 suffer interference from UAV 2's signal. We take the users covered by UAV 1 as an example to explain how to place adjacent UAVs to ensure they can correctly and sequentially decode the signals from UAV 1 and the BS.

1) Constraint for Decoding UAV Signal: Take Fig. 3 as an example. A is the closest point to the BS at the edge of UAV 1's coverage. Suppose UAVs 1 and 2 are deployed at $l_{j,k}$ and $l_{j',k'}$. The channel gain from UAV 1 ($l_{j,k}$) to point A is the minimum signal gain to the coverage edge, calculated as

$$g_{j,k}^{(min)} = 10^{-\frac{f(\theta)\phi\left(R_{j,k},z_{j,k}\right)}{10}}.$$

The channel gain from the BS to point A is the maximum signal gain to the edge of UAV 1's coverage, calculated as

$$g_{m,j,k}^{(max)} = 10^{-\frac{\left(\sqrt{\left(h_{m,j}-R_{j,k}\right)^2+z_m^2}\right)^{\gamma}}{10}}$$

where $h_{j,m} = \sqrt{(x_j-x_m)^2 + (y_j-y_m)^2}$ is the horizontal distance between UAV 1 ($l_{j,k}$) and the BS, and α is the path loss exponent. p_u and p_m represent the transmit power of UAV and BS, respectively. If the received signal power from the BS at point A is lower than that from UAV 1, the received signal power from BS is lower than that from UAV 1 within UAV 1's coverage. Devices covered by UAV 1 can decode/reconstruct the signal from this UAV and perform interference cancellation if and only if

$$p_m g_{j,k,m}^{(max)} < p_u g_{j,k}^{(min)}. \tag{5}$$

2) Constraint for Decoding BS Signal: Because of spectrum reuse, users within UAV 1's coverage suffer interference from UAV 2's signal. In Fig. 3, B is the closest to UAV 2 at the edge of UAV 1's coverage. The channel

gain from UAV 2 to point B is the maximum channel gain within UAV 1's coverage, calculated as

$$g_{j',k',j,k}^{(max)} = 10^{-\frac{f(\theta)\phi\left(h_{j',j}-R_{j,k},z_{j',k'}\right)}{10}}$$

where $d_{j,j'} = \sqrt{(x_j-x_{j'})^2+(y_j-y_{j'})^2}$ is the horizontal distance between the two UAVs. C is the farthest point from macro BS at the edge of UAV 1's coverage. The channel gain from the BS to point C is the minimum channel gain within UAV 1's coverage, calculated as

$$g_{m,j,k}^{(min)} = 10^{-\frac{\left(\sqrt{\left(h_{m,j}+R_{j,k}\right)^2+z_m^2}\right)^{\gamma}}{10}}.$$

If the interference signal power from UAV 2 received at point B is lower than that from BS received at point C, all interference signals within UAV 1's coverage are lower than the BS signal. Therefore, for the UAVs located at $l_{j,k}$ and $l_{j',k'}$, users under UAV 1's coverage can decode and reconstruct the signal from BS, if and only if inequality (6) is satisfied.

$$p_u g_{j',k',j,k}^{(max)} < p_m g_{j,k,m}^{(min)}. \tag{6}$$

C. Video Layer Reception and Decoding Framework

Constraints (5) and (6) ensure that users covered by a UAV can receive the base layer from the UAV and the enhancement layer sent by the BS. The set of users in multicast group n covered by a UAV at $l_{j,k}$ is denoted as $\mathcal{I}_{j,k,n}$. 0-1 variable $q_{j,k,n} = 1$ indicates the association between a UAV at $l_{j,k}$ and multicast group n, 0 otherwise. By receiving signals from the UAV at $l_{j,k}$, users in $\mathcal{I}_{j,k,n}$ suffer interference from the BS and other UAVs associated with multicast group n. Suppose the bandwidth of each subchannel is e, and b_n subchannels are allocated to multicast group n. The achievable rate of user $i \in \mathcal{I}_{j,k,N}$ to decode the signal from the UAV at $l_{j,k}$ is represented as (7) at the bottom of the next page, a function of b_n and $q_{j,k,n}$, where σ^2 denotes the average background noise power.

Constraint (6) ensures that, except for UAV at $l_{j,k}$, the interference signal strengths from other UAVs are lower than the signal strength from BS. When decoding the BS signal, users suffer interference from distant UAV signals. The achievable rate of ground device $i \in \mathcal{I}_{j,k,n}$ to decode the BS signal is a function of b_n and $q_{j,k,n}$, i.e.,

$$r_{m,n,i}(b_n, \mathcal{Q}_n)$$
$$= b_n e \log_2\left(1 + \frac{p_m g_{m,i}}{\sum_{j' \in \mathcal{J}/\{j\}} \sum_{k' \in \mathcal{K}_j/\{k\}} q_{j',k',n} p_u g_{j',k',i} + \sigma^2}\right). \tag{8}$$

For the devices in group n, the minimum bitrates to decode the base layer and the enhancement layer is denoted as λ_1^n and λ_3^n, corresponding to

$$r_{j,k,n,i}(b_n, \mathcal{Q}_n) \geq \lambda_{1,n} \tag{9}$$

and

$$r_{m,n,i}(b_n, \mathcal{Q}_n) \geq \lambda_{2,n}. \tag{10}$$

(a) Example of multicast group 1 associated with UAV 1.

(b) Example of multicast group 2 associated with UAVs 1 and 2.
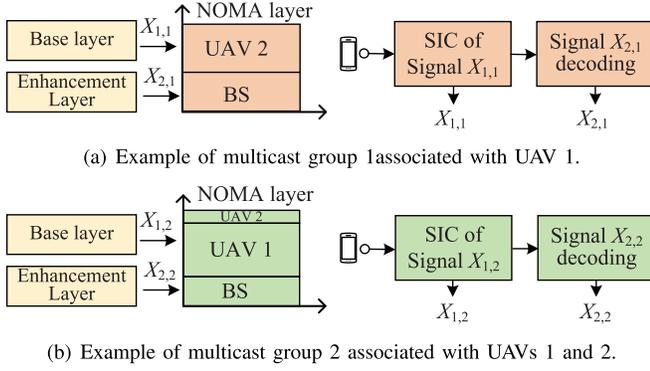
Fig. 4. Signal superposition and SIC under different associated patterns.

The prerequisite for receiving and reconstructing the enhancement layer is receiving the base layer. Device i can decode the enhancement layer if (9) and (10) are satisfied simultaneously.

We now explain the superposition coding in the power domain of UAV and BS signals and the interference cancellation under constraints (5) and (6). Still taking Fig. 1 as an example, two possible UAV-group association cases are considered:

1) Each Multicast Group Is Associated With a Unique UAV (See Fig. 4(a)): Multicast group 1 is only associated with UAV 2. Users under UAV 2's coverage receive signals from UAV 2 stronger than those from BS. The base layer signal, $X_{1,1}$, and enhancement layer signal, $X_{2,1}$, are propagated through the transmit power of UAV 2 and the BS, respectively. As long as the reception rate of ground devices under UAV 2's coverage satisfies (5) and (6), $X_{1,1}$ and $X_{2,1}$ can be decoded via interference cancellation.

2) One Multicast Group Is Associated With Multiple UAVs (See Fig. 4(b)): Multicast group 2 is associated with both UAVs 1 and 2. Users covered by UAV 1 in group 2 are far from UAV 2. They receive signals from UAV 1 stronger than those from BS and suffer interference from UAV 2, weaker than BS signals. The base layer signal $X_{1,2}$ is propagated through the transmit power of UAV 1, and the enhancement layer signal $X_{2,2}$ relies on BS. If the reception rates of users covered by UAV 1 satisfy (5) and (6), they can decode $X_{1,2}$ and $X_{2,2}$ through SIC without further interference cancellation.

III. VIDEO QUALITY MAXIMIZATION PROBLEM

A. Graph Model Construction

It is known from Section II-C that UAV deployment and multicast group association affect superposition coding and interference cancellation of UAV and BS signals. This section constructs a visualizable graph model to characterize the coupling among different decision variables, assisting UAV deployment and UAV-group association.

By performing the mean-shift clustering algorithm [34] on BS-edge users, we obtain a group of candidate UAV locations, denoted as $\mathcal{J}$. Let $\mathcal{G} = (\mathcal{V}, \mathcal{E})$ denote an undirected graph, where each vertex corresponds to a candidate decision on UAV placement and multicast group association that meets constraint (5). Thus, the vertex set can be expressed as

$$\mathcal{V}(\mathcal{G}) = \left\{ v_{j,k,n} | p_m g_{j,k,m}^{(\max)} < p_u g_{j,k}^{(\min)} j \in \mathcal{J}, k \in \mathcal{K}_j, n \in \mathcal{N} \right\} \tag{11}$$

where $\mathcal{N}$ is the set of multicast groups.

When two UAVs located at $l_{j,k}$ and $l_{j',k'}$ are both associated with multicast group n, the constraint corresponding to (6) is re-expressed as

$$\begin{cases} p_u g_{j',k',j,k}^{(\max)} < p_m g_{j,k,m}^{(\min)}, l_{j,k} \neq l_{j',k'}, \ n = n' \\ p_u g_{j,k,j'}^{(\max)} < p_m g_{j',k',m}^{(\min)}, l_{j,k} \neq l_{j',k'}, n = n'. \end{cases} \tag{12}$$

Regardless of the association pattern, a hovering UAV at (x_j, y_j) can only choose a unique height index k, corresponding to

$$l_{j,k} = l_{j',k'}, j = j'. \tag{13}$$

An edge exists between $v_{j,k,n}$ and $v_{j',k',n'}$ if and only if (12) or (13) holds. Accordingly, the edge set is expressed as

$$\mathcal{E}(\mathcal{G}) = \left\{ \left(v_{j,k,n}, v_{j',k',n'} \right) \in \mathcal{V}(\mathcal{G}) | (12) \text{ or } (13) \right\}. \tag{14}$$

A clique $\mathcal{C} \subseteq \mathcal{V}$ is a subset of vertices in $\mathcal{G}$ where every two vertices are connected. Each clique can be mapped to a group of decision variables for UAV deployment and UAV-group association.

B. Case Analysis

To facilitate an understanding of graph generation and clique selection, we provide an example with multicast groups 1 and 2. The candidate UAV locations include $l_{1,1}$, $l_{1,2}$, and $l_{2,2}$. Assume the channel gains from the BS to ground devices and those from candidate UAV locations to ground devices satisfy the following conditions:

(i) $p_m g_{1,1,m}^{(\max)} < p_u g_{1,1}^{(\min)}$;

(ii) $p_m g_{1,2,m}^{(\max)} < p_u g_{1,2}^{(\min)}$;

(iii) $p_m g_{2,2,m}^{(\max)} < p_u g_{2,2}^{(\min)}$;

(iv) $p_u g_{2,2,1,1}^{(\max)} < p_m g_{1,1,m}^{(\min)}, p_u g_{1,1,2,2}^{(\max)} < p_m g_{2,2,m}^{(\min)}$, $l_{1,1} \neq l_{2,2}$;

(v) $p_u g_{2,2,1,2}^{(\max)} > p_m g_{1,2,m}^{(\min)}, p_u g_{1,2,2,2}^{(\max)} > p_m g_{2,2,m}^{(\min)}$, $l_{1,2} \neq l_{2,2}$.

Substituting (i), (ii), and (iii) into (11), we generate a vertex set as

$$\mathcal{V}(\mathcal{G}) = \left\{ v_{1,1,1}, v_{1,1,2}, v_{1,2,1}, v_{1,2,2}, v_{2,2,1}, v_{2,2,2} \right\}.$$

$$r_{j,k,n,i}(b_n, \mathcal{Q}_n) = b_n e \log_2 \left(1 + \frac{q_{j,k,n} p_u g_{j,k,i}}{\sum\limits_{j' \in \mathcal{J}/\{j\}} \sum\limits_{k' \in \mathcal{K}_j/\{k\}} q_{j',k',n} p_u g_{j',k',i} + p_m g_{m,i} + \sigma^2} \right) \tag{7}$$
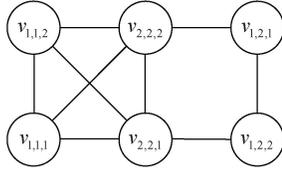
Fig. 5. Graph model example.

(a) Cliques with one vertex.

(b) Cliques with two vertices

(c) Cliques of three vertices

(d) Clique of four vertices
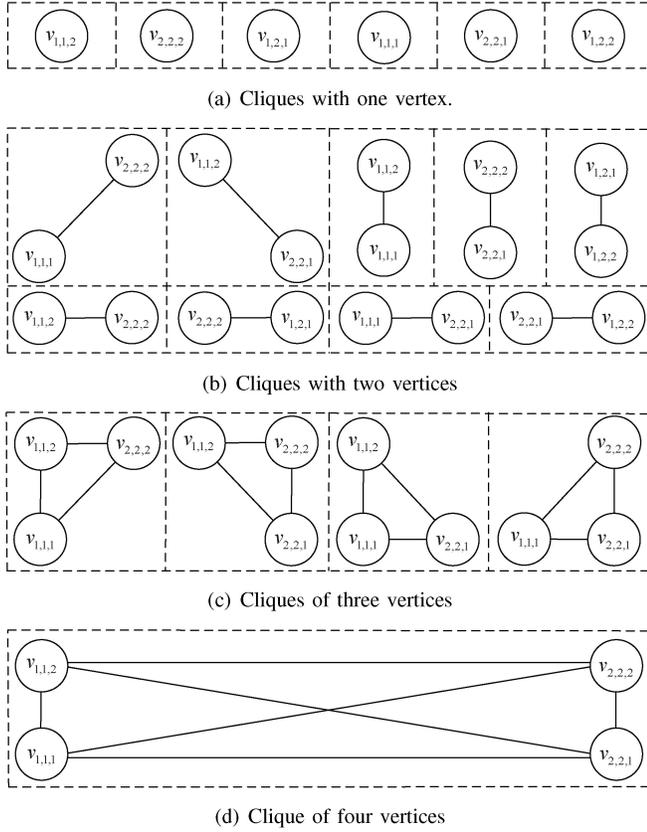
Fig. 6. Examples of Cliques with different sizes.

Since condition (iv) satisfies (12), an edge exists between vertices $v_{1,1,2}$ and $v_{2,2,2}$, $v_{1,1,1}$ and $v_{2,2,1}$. In contrast, vertex pairs $(v_{1,2,2}, v_{2,2,2})$ and $(v_{1,2,1}, v_{2,2,1})$ have no edge because condition (v) does not meet (12). $l_{1,1}$ and $l_{1,2}$ have different flight heights, violating (13). Thus, vertex pairs $(v_{1,2,1}, v_{1,1,2})$, $(v_{1,2,1}, v_{1,1,1})$, $(v_{1,2,2}, v_{1,1,1})$, and $(v_{1,2,2}, v_{1,1,2})$ have no edge. Accordingly, the edge set in this case is

$$\mathcal{E}(G) = \Big\{ (v_{1,1,1}, v_{1,1,2}), (v_{2,2,2}, v_{2,2,1}), (v_{1,2,1}, v_{1,1,2}),$$
$$(v_{1,1,2}, v_{2,2,2}), (v_{2,2,2}, v_{1,2,1}), (v_{1,1,1}, v_{2,2,1}),$$
$$(v_{2,2,1}, v_{1,2,2}), (v_{1,1,2}, v_{2,2,1}), (v_{1,1,1}, v_{2,2,2}) \Big\}.$$

Fig. 5 represents the graph model built based on $\mathcal{V}$ and $\mathcal{E}$. Let C denote the number of vertices of clique $\mathcal{C}$. Next, we classify the cliques by C, as shown in Fig. 6 to explain the impact of the number of available UAVs (denoted by α) on clique selection:

1) Case of $C = 1$ shown in Fig. 6(a): Clique $\{v_{1,1,1}\}$ means one UAV is placed at $l_{1,1}$ serving multicast group 1,

while Clique $\{v_{1,2,2}\}$ represents one UAV is placed at $l_{1,2}$ serving multicast group 2.

2) Case of $C = 2$ shown in Fig. 6(b): By observation, some cliques (e.g., $\{v_{1,1,2}, v_{1,1,1}\}$ and $\{v_{2,2,2}, v_{2,2,1}\}$) contain a single deployment location, others (e.g., $\{v_{2,2,2}, v_{1,1,1}\}$ and $\{v_{2,2,2}, v_{1,2,1}\}$) have two candidate locations. When $\alpha = 1$, clique $\{v_{1,1,1}, v_{1,1,2}\}$ means placing one UAV at $l_{1,1}$ serving both group 1 and 2. If $\alpha = 2$, option $\{v_{1,1,1}, v_{2,2,2}\}$ is placing one UAV at $l_{1,1}$ for group 1 and another at $l_{2,2}$ for group 2.

3) Case of $C = 3$ shown in Fig. 6(c): Since each clique contains two optional deployment locations (i.e., $l_{1,1}$ and $l_{2,2}$), this case requires two UAVs. If $\alpha = 2$ and clique $\{v_{1,1,1}, v_{1,1,2}, v_{2,2,2}\}$ is selected, one UAV is placed at $l_{1,1}$ and associated with groups 1 and 2, and another UAV is set at $l_{2,2}$ serving group 2. Similarly, in the case of $\alpha = 2$ and clique $\{v_{1,1,2}, v_{2,2,2}, v_{2,2,1}\}$, one UAV is deployed at $l_{1,1}$ and associated with group 2, and another UAV is set at $l_{2,2}$ serving groups 1 and 2.

4) Case of $C = 4$ shown in Fig. 6(d): Similar to the previous case, since the clique of four vertices only contains two deployment positions, up to two UAVs may be used in this case. If $\alpha = 2$ and clique $\{v_{1,1,1}, v_{1,1,2}, v_{2,2,2}, v_{2,2,1}\}$ is chosen, placing one UAV at $l_{1,1}$ associated with groups 1 and 2, and the other UAV is placed at $l_{2,2}$ to serve groups 1 and 2.

From the above examples, the chosen clique determines available deployment positions. The selection of a clique must consider available UAVs and optional deployment locations. The number of UAVs dispatched shall not exceed the number of optional deployment locations. When the number of UAVs exceeds the available deployment locations, the corresponding clique becomes unavailable due to the inability to find enough UAVs. For instance, the clique in Fig. 6(d) requires two UAVs, which cannot be selected for $\alpha < 2$

C. Problem Formulation

The video quality maximization problem is transformed into a clique-based spectrum partitioning problem, essentially finding a clique to determine the UAV placement, association patterns, and each multicast group's subchannel numbers.

Define $q_{j,k,n}$ to indicate whether $v_{j,k,n}$ is included in the selected clique $\mathcal{C}$.

$$q_{j,k,n} = \begin{cases} 1, & \text{if } v_{j,k,n} \in \mathcal{C} \\ 0, & \text{otherwise} \end{cases} \quad (15)$$

Each clique corresponds to a candidate UAV placement and UAV-group association plan.

Let 0–1 variables $u_{1,n,i}$ and $u_{2,n,i}$ represent whether user i in multicast group n can receive/decode the base layer and the enhancement layer, respectively. The aggregated PSNR of videos received by multicast group n is expressed as a function of b_n and $\mathcal{Q}_n = \bigcup_{j \in \mathcal{J}, k \in \mathcal{K}} q_{j,k,n}$, i.e.,

$$f_n(b_n, \mathcal{Q}_n) = \sum_{i \in \mathcal{I}_n} (u_{1,n,i} - u_{2,n,i}) \text{PSNR}_{1,n}$$
$$+ \sum_{i \in \mathcal{I}_n} u_{2,n,i} \text{PSNR}_{2,n}. \quad (16)$$

By applying (16) to all groups in $\mathcal{N}$, the video quality maximization problem is modeled as $\mathcal{P}1$.

$$\mathcal{P}1 : \max_{\{b_n, \mathcal{Q}_n\}_{n \in \mathcal{N}}} \sum_{n \in \mathcal{N}} f_n(b_n, \mathcal{Q}_n)$$

$$s.t. \begin{cases} q_{j,k,n} + q_{j',k',n'} = 1, \forall (v_{j,k,n}, v_{j',k',n'}) \notin \mathcal{E}(\mathcal{G}) & (17\text{a}) \\[4pt] \sum_{j \in \mathcal{J}} \sum_{k \in \mathcal{K}} \text{sgn}\Big(\sum_{n \in \mathcal{N}} q_{j,s,n}\Big) \leq \alpha & (17\text{b}) \\[4pt] r_{m,n,i}(b_n, \mathcal{Q}_n) - \varsigma u_{1,n,i} \leq \lambda_{1,n}, \forall n \in \mathcal{N}, i \in \mathcal{I}_{j,k,n} & (17\text{c}) \\[4pt] r_{m,n,i}(b_n, \mathcal{Q}_n) + \varsigma(1 - u_{1,n,i}) \geq \lambda_{1,n}, \\ \forall n \in \mathcal{N}, i \in \mathcal{I}_{j,k,n} & (17\text{d}) \\[4pt] r_{j,k,n,i}(b_n, \mathcal{Q}_n) - \vartheta u_{2,n,i} u_{1,n,i} \leq \lambda_{2,n}, \\ \forall v_{j,k,n} \in \mathcal{V}(\mathcal{G}), i \in \mathcal{I}_{j,k,n} & (17\text{e}) \\[4pt] r_{j,k,n,i}(b_n, \mathcal{Q}_n) + \vartheta(1 - u_{2,n,i}) u_{1,n,i} \geq \lambda_{2,n}, \\ \forall v_{j,k,n} \in \mathcal{V}(\mathcal{G}), i \in \mathcal{I}_{j,k,n} & (17\text{f}) \\[4pt] \sum_{n \in \mathcal{N}} b_n \leq B & (17\text{g}) \\[4pt] q_{j,k,n} \in \{0, 1\}, \forall v_{j,k,n} \in \mathcal{V}(\mathcal{G}) & (17\text{h}) \\[4pt] u_{a,n,i} \in \{0, 1\}, \forall n \in \mathcal{N}, a \in \{1, 2\}, i \in \mathcal{I}_{j,k,n} & (17\text{i}) \end{cases}$$

Constraint (17a) means that if vertices $v_{j,k,n}$ and $v_{j',k',n'}$ have no edge, they do not belong to the same clique. Constraint (17b) allows a UAV to serve multiple groups, which contains an indicative function, $\text{sgn}(\cdot)$, calculating the number of UAVs required by clique $\mathcal{C}$, which should not be larger than the available UAV number, α. When a UAV placed at $l_{j,k}$ is not associated with any multicast group, $\text{sgn}(\sum_{n \in \mathcal{N}} q_{j,k,n})$ is set to 0, otherwise 1. In (17c) and (17d), ς is a sufficiently large constant to ensure

$$u_{1,n,i} = \begin{cases} 1, & r_{m,n,i}(b_n, \mathcal{Q}_n) - \lambda_{1,n} > 0 \\ 0, & r_{m,n,i}(b_n, \mathcal{Q}_n) - \lambda_{1,n} \leq 0. \end{cases} \quad (18)$$

Under $u_{1,n,i} = 1$ ($u_{1,n,i} = 0$), ground device i can (cannot) receive/decode the base layer. ϑ in (17e) and (17f) is also a sufficiently large constant to guarantee

$$u_{2,n,i} = \begin{cases} 1, & \big(r_{j,k,n,i}(b_n, \mathcal{Q}_n) - \lambda_{2,n}\big) u_{1,n,i} > 0 \\ 0, & \big(r_{j,k,n,i}(b_n, \mathcal{Q}_n) - \lambda_{2,n}\big) u_{1,n,i} \leq 0. \end{cases} \quad (19)$$

When $u_{1,n,i} = 1$, $u_{2,n,i} = 1$ ($u_{2,n,i} = 0$) means user i can (cannot) receive and decode the enhancement layer. The subchannels allocated to groups should not exceed B available at BS, ensured by (17g).

Due to the strong coupling among UAV placement, UAV-group association patterns, and subchannel allocation, solving $\mathcal{C}$ encounters high computational complexity, especially when $|\mathcal{V}(\mathcal{G})|$ are large. Therefore, problem decoupling and efficient algorithm design are inevitable.

IV. ALGORITHM DESIGN

$\mathcal{P}1$ is decoupled into 1) the UAV placement and UAV-group association subproblem and 2) the subchannel allocation subproblem. A branch-and-bound-based maximum weight clique algorithm solves the former, and the latter is solved through a lightweight matching policy.

Algorithm 1: Search_Clique $(\mathcal{G}(\mathcal{V}, \mathcal{E}), \mathcal{V}', \mathcal{C}, \mathcal{C}')$

1   **if** $\mathcal{V}' = \emptyset$ **then**
2     $\lfloor$ **return** $\mathcal{C}$;
3   $\mathcal{E}' \leftarrow \big\{(v_{j,k,n}, v_{j',k',n'}) \in \mathcal{V}' |(12) \text{ or } (13)\big\}$;
4   $t \leftarrow \text{get\_upper\_bound}(\mathcal{G}(\mathcal{V}', \mathcal{E}'))$;
5   **if** $\sum_{v_{j,k,n} \in \mathcal{C}} w_{j,k,n} + t < \sum_{v_{j,k,n} \in \mathcal{C}'} w_{j,k,n}$ **then**
6     $\lfloor$ **return** $\mathcal{C}'$;
7   **while** $\mathcal{V}' \neq \emptyset$ **do**
8     $j^*, k^*, n^* \leftarrow \arg \max_{v_{j,k,n} \in \mathcal{V}'} w_{j,k,n}$;
9   **if** $\text{get\_drone\_num}(\mathcal{C} \cup \{v_{j^*,k^*,n^*}\}) > \alpha$ **then**
10       $\mathcal{V}' \leftarrow \mathcal{V}' \backslash \{v_{j^*,k^*,n^*}\}$;
11   Continue;
12     $\mathcal{V}'' \leftarrow \Gamma(v_{j^*,k^*,n^*}) \cap \mathcal{V}'$;
13     $\mathcal{C}'' \leftarrow \text{get\_clique}(\mathcal{G}(\mathcal{V}, \mathcal{E}), \mathcal{V}'', \mathcal{C} \cup \{v_{j^*,k^*,n^*}\}, \mathcal{C}')$;
14   **if** $\sum_{v_{j,k,n} \in \mathcal{C}''} w_{j,k,n} > \sum_{v_{j,k,n} \in \mathcal{C}'} w_{j,k,n}$ **then**
15       $\lfloor$ $\mathcal{C}' \leftarrow \mathcal{C}''$;
16     $\mathcal{V}' \leftarrow \mathcal{V}' \backslash \{v_{j^*,k^*,n^*}\}$;
17 **return** $\mathcal{C}'$;

A. Subproblem 1: UAV Placement and UAV-Group Association

The weight of vertex $v_{j,k,n}$ is defined as

$$w_{j,k,n} \triangleq f_n(\hat{b}_n, \mathcal{Q}_n), \hat{b}_n = 1 \quad (20)$$

to reflect the contribution of vertex $v_{j,k,n}$ to the aggregated PSNR of videos received when $b_n = 1$ subchannel is allocated to multicast group n. On this basis, the UAV deployment and multicast group association subproblem is transformed into a maximum weight clique problem with vertex number constraints as follows

$$\mathcal{P}1.1 \max_{\{\mathcal{Q}_n\}_{n \in \mathcal{N}}} \sum_{v_{j,k,n} \in \mathcal{V}} q_{j,k,n} w_{j,k,n}$$

$$\text{s.t.} \quad (17\text{a}), (17\text{b}), (17\text{c}), (17\text{d}), (17\text{e}), (17\text{f}), (17\text{h}), (17\text{i})$$

As analyzed in Section III-B, the clique selection is constrained by the number of available UAVs, without the correspondence with the required number of UAVs, which prevents the use of maximum clique or maximum weight clique algorithms [35]. Another possibility is the maximum k-clique or maximum weight-k-clique algorithms [36]. Both algorithms output cliques of k, while the size of clique $\mathcal{C}$ output by $\mathcal{P}1.1$ is unknown. Considering these specifics, an improved branch-and-bound-based maximum weight clique algorithm is developed with details in Algorithm 1, considering the UAV number constraint.

Initially, $\mathcal{C}'$ and $\mathcal{C}$ are set to empty, $\mathcal{V}'$ contains all vertices in graph $\mathcal{G}$. Before clique search, $\mathcal{G}(\mathcal{V}', \mathcal{E}')$ is input into the bounding procedure, get_upper_bound (), to obtain the weight value of the maximum weight clique, denoted by t, which serves as the upper bound of that for subgraphs (line 4). If the upper bound of $\mathcal{V}_{rest}$ is not larger than the current maximum weight clique $\mathcal{C}'$, the recursive search on

$\mathcal{G}(\mathcal{V}', \mathcal{E}')$ terminates and returns $\mathcal{C}'$ (lines 5 and 6). Otherwise, vertex v_{j^*,k^*,n^*} with the maximum weight is selected from $\mathcal{V}'$. Function get_drone_num($\mathcal{C} \cup \{v_{j^*,k^*,n^*}\}$) checks the number of UAVs required by clique $\mathcal{C} \cup \{v_{j^*,k^*,n^*}\}$. If it exceeds α, skip the search at this point; otherwise, add it to $\mathcal{C}$. Then the adjacent vertices of v_{j^*,k^*,n^*}, obtained by function $\Gamma(v_{j^*,k^*,n^*})$, in $\mathcal{V}'$ constitute the new candidate set $\mathcal{V}''$. Recursively call Algorithm 1 on $\mathcal{G}(\mathcal{V}', \mathcal{E}')$ (lines 12 and 13). If the returned clique $\mathcal{C}''$ from $\mathcal{G}(\mathcal{V}', \mathcal{E}')$ has larger weight than $\mathcal{C}'$, update $\mathcal{C}'$ as $\mathcal{C}''$ and remove v_{j^*,k^*,n^*} from $\mathcal{V}'$ (lines 14-16). Continue the search for qualified vertices until $\mathcal{V}'(\mathcal{G})$ becomes empty, and return $\mathcal{C}'$.

Combining $\mathcal{C}'$ with (15), we obtain the solution of subproblem $\mathcal{P}1.1$ as $\mathcal{Q}^* = \bigcup_{n \in \mathcal{N}} \mathcal{Q}_n^*$, where $\mathcal{Q}_n^* = \bigcup_{j \in \mathcal{J}, k \in \mathcal{K}} q_{j,k,n}^*$. The bounding procedure prunes branches of vertices that violate the upper limit, thus reducing the size of the whole search tree. Furthermore, observing a clique's required number of UAVs avoids unnecessary computations. In the worst case, the complexity of searching all vertices is $O(|\mathcal{V}(\mathcal{G})|2^{|\mathcal{V}(\mathcal{G})|})$.

B. Subproblem 2: Subchannel Allocation

Given the output of Algorithm 1, the subchannel allocation subproblem is formulated as

$$\mathcal{P}1.2 : \max_{\{b_n\}_{n \in \mathcal{N}}} \sum_{n \in \mathcal{N}} f_n(b_n, \mathcal{Q}_n^*)$$

$$\text{s.t. (17c), (17d), (17e), (17f), (17g), (17i)}$$

The minimum required rates for user $i \in \mathcal{I}_{j,k,n}$ to receive the base layer and enhancement layer are determined by (21) and (22), shown at the bottom of the next page, respectively. When the minimum reception rate requirements for both the base layer and enhancement layer are met, there is no need to increase the subchannels further. The maximum number of subchannels required by multicast group n is determined as

$$b_n^{(\max)} = \max\left\{ \left\lceil \frac{\lambda_{1,n}}{k_{1,n}} \right\rceil, \left\lceil \frac{\lambda_{2,n}}{k_{2,n}} \right\rceil \right\}. \tag{23}$$

To solve $\mathcal{P}1.2$, we design a resource-aware heuristic strategy. Before strategy selection, three possible cases for available subchannels (B) and multicast groups (N) are considered:

1) When $B \leq 2N$, we sort the PSNRs of multicast groups (determined by $f_n(b_n, \mathcal{Q}_n^*)$) in descending order, and assign one subchannel to each of the $B - N$ multicast groups with the highest PSNR values. The computational complexity in this case is $O(n^2)$.

2) When $B \geq N + \sum_{n \in \mathcal{N}} b_n^{(\max)}$, all multicast group users can receive the base and enhancement layers. Multicast group $n \in \mathcal{N}$ is allocated $b_n^{(\max)}$ subchannels with a complexity of $O(1)$;

3) When $2N < B < N + \sum_{n \in \mathcal{N}} b_n^{(\max)}$, an improved knapsack algorithm determines subchannel partitioning. The N multicast groups are seen as N types of items, each with B items. These items need to be put into a knapsack of capacity B. For the nth type, the weight of the b_nth item is b_n, and its profit is determined by $f_n(b_n, \mathcal{Q}_n^*)$. Let the maximum PSNR of the top n multicast groups with the remaining b subchannels be

Parameter	Value
BS height (z_m)	10m
BS transmit power (p_m)	30W
UAV transmit power (p_u)	2W
Candidate UAV flight heights ($z_{j,k}$)	50m, 80m
Carrier frequency (c)	3.5GHz [37]
LoS threshold (ξ)	0.5
Free space loss threshold (ψ)	89dB
Average noise power (σ^2)	-174 dBm/Hz
UAV parameters (a, o, η_{LoS}, η_{NLoS})	(9.61, 0.16, 1, 20)
Orthogonal subchannel bandwidth (w)	50 kHz
Number of subchannels (B)	5-12
Number of multicast groups (N)	3-5
Number of users in group n (I_n)	35

$F(n, b)$. If $b \geq b_n^{(\max)}$, $[0, b_n^{(\max)}]$ subchannels are allocated to group n. Improper numbers of subchannels can be filtered according to rule (24) at the bottom of the next page to reduce unnecessary computations. By recursively solving the maximum PSNRs of the first n groups, the final subchannel allocation that maximizes the aggregated PSNRs is obtained. For each recursion, traversing all cases has a computational complexity of $O(B)$. In the worst case, the complexity of the whole loop is $O(NB^2)$. Simple cases would be complicated without the above classification, increasing the computation burden. The proposed policy can obtain near-optimal solutions at low cost.

V. PERFORMANCE EVALUATION

Simulation experiments are designed on the MATLAB platform to validate the effectiveness of the proposed scheme. We consider a scenario where multiple UAVs collaborate with a macro BS. A real video trace from [38], composed of 10 standard video test sequences with different video layers and each video layer's average bite rate and PSNR is utilized to make the simulations close to an actual scene. BS coverage radius was set to 900m. The video quality improvement of users at BS-edge (the annular region of 750-900m from BS) of BS coverage is evaluated. Detailed parameter settings are listed in Table II.

The proposed methods are categorized into Proposed-1, Proposed-2, and Proposed-3 as specified in Table III. Three baselines are chosen for comparison as described in Table IV.

A. Impact of the Available Number of UAVs

In Fig. 7 and Fig. 7, the aggregated PSNR of Proposed-1 proliferates as B increases from 5 to 11 and becomes stable afterward when $B = 11$. Due to the UAV deployment and multicast group association strategy, the proposed scheme can adapt to insufficient resources with the left turning point. In Baseline-1, where each multicast group associates with only one UAV, the potential for performance growth is limited even with increased B. Proposed-1 controls the interference among UAVs within an acceptable range so that the gain of resource reuse is greater than the interference impact. Compared to

TABLE III
IMPLEMENT OF PROPOSED METHODS

Category	UAV deployment & UAV-group association	UAV flight height	Subchannel allocation
Proposed-1	Proposed graph model and Algorithm 1	Adaptive flight height	Strategy in Section IV-B
Proposed-2	Proposed graph model and Algorithm 1	Adaptive flight height	Equal partition for each group
Proposed-3	Proposed graph model and Algorithm 1	Static height for max. coverage	Strategy in Section IV-B

TABLE IV
IMPLEMENT OF BASELINES

Category	Multiple access technique	Base layer sender	Enhancement layer sender	UAV flight altitude	UAV-group association
Baseline-1 [39]	NOMA	UAV	BS	Static altitude for max. coverage	One UAV per group
Baseline-2 [40]	OMA	UAV	BS	Static altitude for max. coverage	Multiple UAVs per group
Baseline-3 [41]	OMA	UAV	UAV	Static altitude for max. coverage	Multiple UAVs per group

Baseline-2, the superposition coding of NOMA in Proposed-1 allows the BS to share spectrum with UAVs to transmit signals without consuming additional spectrum. For all given values of B, the aggregated PSNR of Proposed-1 is higher than OMA schemes. In Baseline-3, the BS must send base and enhancement layers to UAVs for forwarding to users. When $B < 9$, the aggregated PSNR is 0. Proposed-1 can still provide base layer video service to some users when $B < 8$.

The three subfigures in Fig. 7 show the impact of different numbers of UAVs on the total PSNR received by users. The more UAVs are dispatched, the more aggregated PSNR the proposed scheme achieves. In Proposed-1, the UAVs are relatively dispersed, and the interference between UAVs associated with the same multicast group is slight. Thus, UAV placement can select the height with the maximum coverage radius, which gives the same deployment decisions as directly selecting the maximum coverage height for UAVs in Proposed-3. From Figs. 7(a) and (b), the aggregated PSNR of the proposed scheme and Proposed-3 are close. More UAVs help improve resource utilization but also increase co-channel interference. Adjustable flight heights contribute to reducing interference among UAVs.

B. Impact of the Number of Multicast Groups

Fig. 8 shows the effect of the number of multicast groups on users' average PSNR. From Fig. 8(a), in the case of five groups, the average PSNR of the proposed scheme is about twice that of OMA schemes and 8.4% higher than other NOMA baselines. In Table V, the total PSNR received by multicast group 2 using Proposed-1 is approximately 7.9% higher than Proposed-2. When the number of groups is large, the advantage of the proposed schemes over other schemes is more significant. In Table VI, the total PSNR of multicast group 5 received in Proposed-1 is 3.68 times that in Proposed-2. The equal spectrum partitioning in Proposed-2 leads to unsatisfactory video quality for some users in these multicast groups. Excessive spectrum resources are allocated to other multicast groups. Proposed-1 can dynamically allocate subchannels to match the spectrum demand of each group, avoiding resource waste.

As shown in Fig. 9, Z-score normalization, a commonly used data standardization method, analyzes PSNR values in Tables V and VI to make the data comparable. If a specific PSNR value equals the average achieved across all multicast groups, it will be normalized to 0. If it is below (above) the mean, it will be a negative (positive) number. The standard deviation of the original PSNR values of all groups determines the size of a number. All values are between -1.5 and 1.5 on the y-axis. The projection of the proposed scheme, especially proposed-1, on the y-axis, is more concentrated than other methods, indicating that the proposed scheme can improve the video reception quality while considering fairness.

$$k_{1,n}^{(\min)} = e \min_{i \in \mathcal{I}_{j,k,n}} \log_2\left(1 + \frac{q_{j,k,n}^* p_u g_{j,k,i}}{\sum\limits_{j' \in \mathcal{J}/\{j\}} \sum\limits_{k' \in \mathcal{K}/\{k\}} q_{j',k',n}^* p_u g_{j',k',i} + p_m g_{m,i} + \sigma^2}\right) \tag{21}$$

$$k_{2,n}^{(\min)} = e \min_{i \in \mathcal{I}_{j,n}} \log_2\left(1 + \frac{p_m g_{m,i}}{\sum\limits_{j' \in \mathcal{J}/\{j\}} \sum\limits_{k' \in \mathcal{K}/\{k\}} q_{j',k',n}^* p_u g_{j',k',i} + \sigma^2}\right) \tag{22}$$

$$F(n,b) = \begin{cases} \max_{0 \le b_n \le b} F(n-1, b - b_n) + f_n(b_n, \mathcal{Q}_n^*), & \text{if } b < b_n^{(\max)} \\ \max_{0 \le b_n \le b_n^{(\max)}} F(n-1, b - b_n) + f_n(b_n, \mathcal{Q}_n^*), & \text{if } b \ge b_n^{(\max)} \end{cases} \tag{24}$$

TABLE V
AGGREGATE PSNR (DB) RECEIVED BY EACH MULTICAST GROUP (WITH $\alpha = 4$, $N = 4$, AND $B = 12$)

Method	Group 1	Group 2	Group 3	Group 4	Mean	Variance
Baseline-1	419.88	394.92	454.44	207.34	369.145	12231.49
Baseline-2	122.69	366	501.59	269.72	315	25483.41
Baseline-3	855.92	579.5	894	503.54	708.24	38264.07
Proposed-1	909.74	625.29	946.75	503.54	746.33	17799.57
Proposed-2	909.74	579.5	946.75	503.54	734.88	23503.98
Proposed-3	769.78	658.2	719.53	473.92	655.35	16712.75

TABLE VI
AGGREGATE PSNR (DB) RECEIVED BY EACH MULTICAST GROUP (WITH $\alpha = 4$, $N = 5$, AND $B = 12$)

Method	Group 1	Group 2	Group 3	Group 4	Group 5	Mean	Variance
Baseline-1	419.88	366	454.44	207.34	222.6	334.052	12839.46
Baseline-2	131.68	109.34	537.12	355.44	386.86	304.088	32860.86
Baseline-3	921.76	0	929.76	0	0	370.304	257117.47
Proposed-1	979.72	671	984.62	592.4	702.66	786.08	33657.2
Proposed-2	979.72	671	984.62	592.4	190.8	683.71	107407
Proposed-3	839.76	701.5	757.4	562.78	731.4	718.56	10230.32

(a) Case of three UAVs ($\alpha = 3$).   (b) Case of four UAVs ($\alpha = 4$).   (c) Case of five UAVs ($\alpha = 5$).
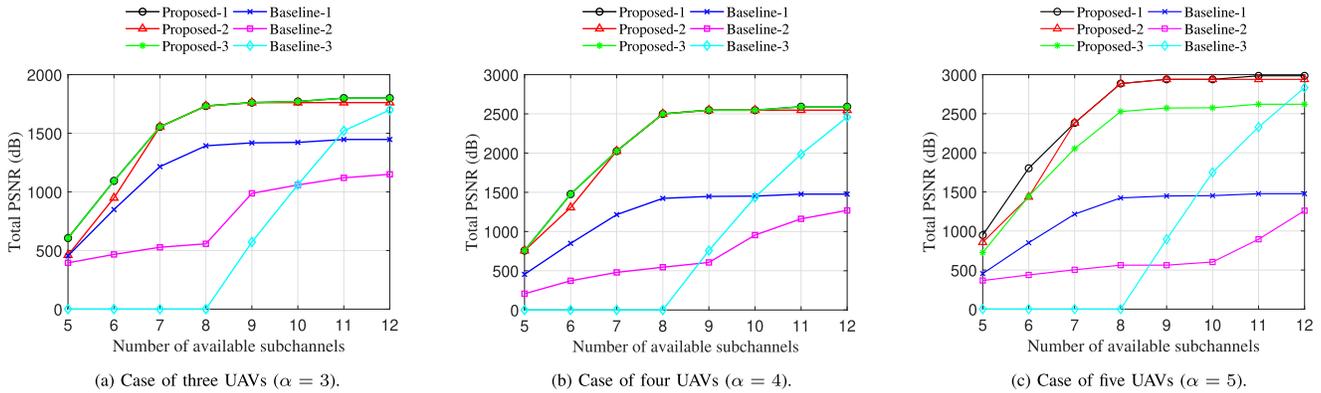
Fig. 7. Aggregated PSNR with varying UAVs in the case of $N = 4$.

(a) Case of three multicast groups ($N = 3$).   (b) Case of four multicast groups ($N = 4$).   (c) Case of five multicast groups ($N = 5$).
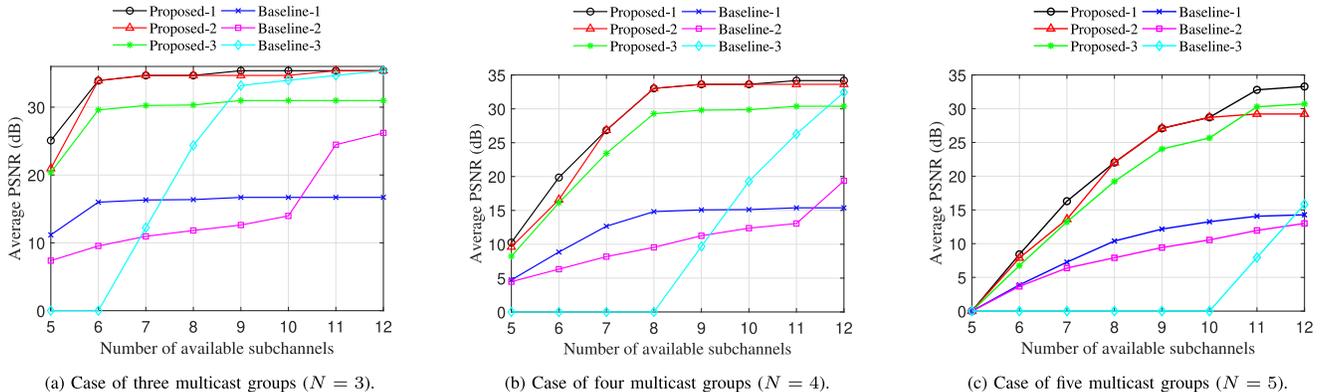
Fig. 8. Average PSNR with varying multicast groups in the case of $\alpha = 6$.

C. Visualization of UAV Deployment

To facilitate the understanding of the proposed clique-based algorithm, we conduct a visual analysis of UAV deployment and UAV-group association patterns. Fig. 10(a) shows the UAV placement in Proposed-3 in the case of $N = 5$ and $\alpha = 4$. When performing Proposed-3, UAVs always select the height of maximum coverage. If two UAVs serving the same multicast group are placed close, the superimposed signals generate interference that negates the benefits of spectral reuse. UAVs 1 and 6 are associated with different multicast groups to reduce interference. The relatively distant UAVs 2 and 3 can associate with the same multicast group. The clique in

(a) Results for Table V.

(b) Results for Table VI.

Fig. 9.   Z-score normalization.

(a) Proposed-3.

(b) Proposed-1
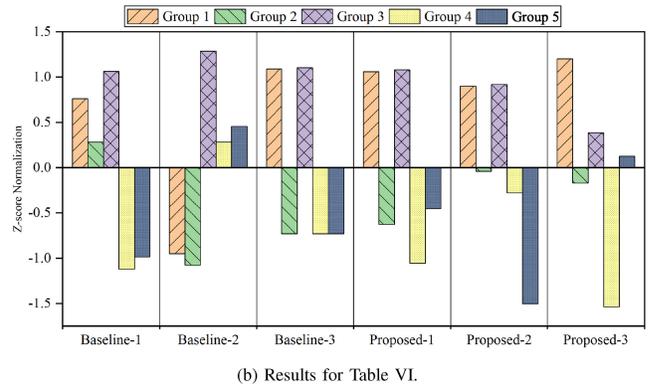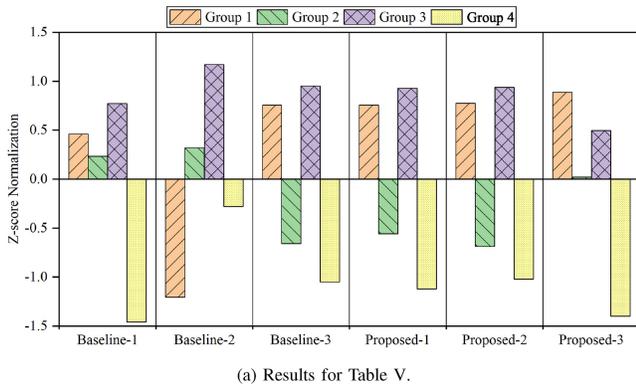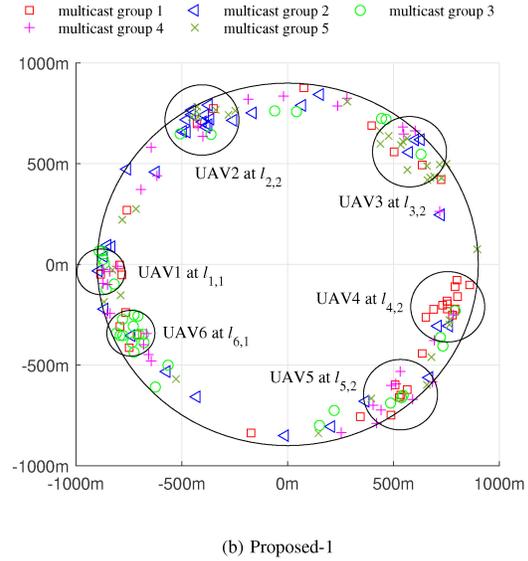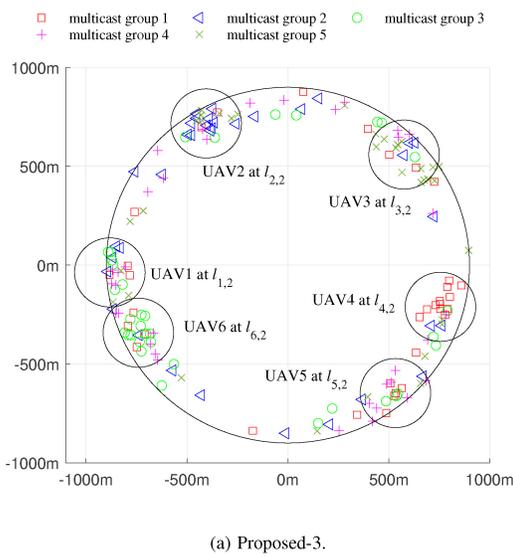
Fig. 10.   UAV deployment and coverage in the case of $\alpha = 6$ and $N = 5$.

(a) Clique generated by Proposed-3.

(b) Clique generated by Proposed-1.
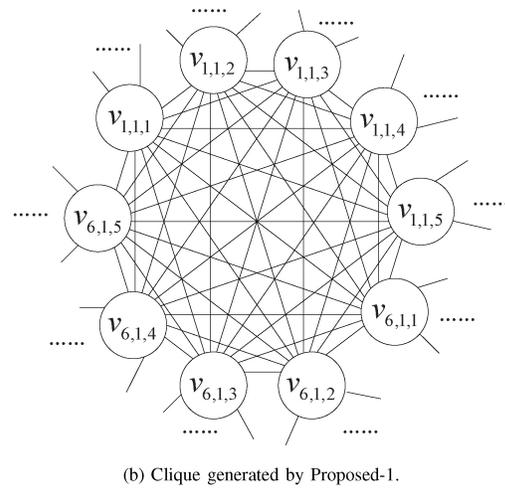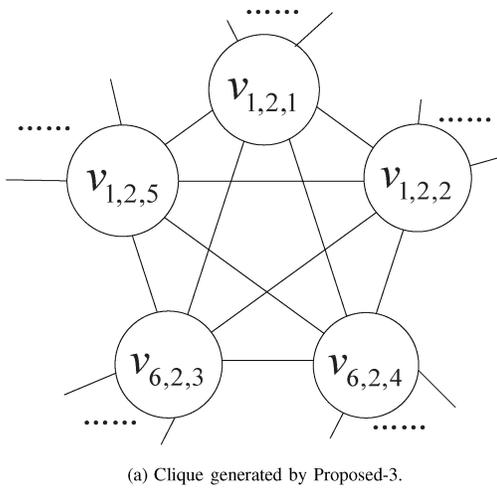
Fig. 11.   UAV deployment and UAV-group association in the form of cliques.

Fig. 11(a) determines the association patterns between UAVs 1, 6, and multicast groups for Fig. 10(a) in the form of a clique determined by Algorithm 1, where UAV 1 is associated with groups 1, 2, and 5, and UAV 6 serves groups 3 and 4. Fig. 10(b) illustrates the UAV placement using Proposed-1 with $N = 5$ and $\alpha = 4$. UAVs associated with the same multicast group can reduce interference by height adjustment, which differs from what happens when using Proposed-3.

Each UAV can serve multiple multicast groups in different subchannels, as shown in Fig. 11(b) abstracted as a clique.

A vertex in the graph model binds an x-y plane projection position and a flight height. The graph initialized by Proposed-1 contains more vertices and edges than Proposed-2 because the former supports flight height adaptation. The number of vertices and edges is proportional to the number of optional flight altitudes. More vertices and edges increase the decision space of Algorithm 1 for capturing a more matching clique to decide on UAV deployment and UAV-group association, with a higher PSNR for video reception than other schemes.

VI. Conclusion

In this paper, we have proposed a NOMA-enabled real-time SVC multicasting framework based on UAV relays. The goal is to improve the video reception quality of users in BS-edge areas. A visualizable graph model is constructed to characterize the coupling among different decision variables. Based on the graph model, the joint optimization of UAV deployment, UAV-group association, and subchannel allocation is modeled as an integer nonlinear programming problem. A clique-based search algorithm and a heuristic policy are used in problem-solving. Simulation results have confirmed the superiority and effectiveness of the proposed scheme. In addition to providing video multicast, the proposed framework has the potential to be further applied in UAV swarm deployment and UAV-assisted mobile edge caching. Our future work will investigate UAV-assisted video multicasting in rate-splitting multiple access networks and explore improving UAV services' security and environmental adaptability based on blockchain and AI.

References

[1] H.-H. Liu and H.-Y. Wei, "5G NR multicast and broadcast QoS enhancement with flexible service continuity configuration," *IEEE Trans. Broadcast.*, vol. 68, no. 3, pp. 689–703, Sep. 2022.

[2] P. Ji, J. Jia, J. Chen, L. Guo, A. Du, and X. Wang, "Reinforcement learning based joint trajectory design and resource allocation for RIS-aided UAV multicast networks," *Comput. Netw.*, vol. 227, Art. no. 109697, May 2023.

[3] A. Ksentini and T. Taleb, "QoE-oriented adaptive SVC decoding in DVB-T2," *IEEE Trans. Broadcast.*, vol. 59, no. 2, pp. 251–264, Jun. 2013.

[4] M. F. Sohail, C. Y. Leow, and S. Won, "Energy-efficient non-orthogonal multiple access for UAV communication system," *IEEE Trans. Veh. Technol.*, vol. 68, no. 11, pp. 10834–10845, Nov. 2019.

[5] E. Iradier et al., "Using NOMA for enabling broadcast/unicast convergence in 5G networks," *IEEE Trans. Broadcast.*, vol. 66, no. 2, pp. 503–514, Jun. 2020.

[6] H. Duan, Y. Zhang, and J. Song, "Block-level utility maximization for NOMA-based layered broadcasting," *IEEE Trans. Broadcast.*, vol. 66, no. 1, pp. 21–33, Mar. 2020.

[7] H. Wu, Z. Wei, Y. Hou, N. Zhang, and X. Tao, "Cell-edge user offloading via flying UAV in non-uniform heterogeneous cellular networks," *IEEE Trans. Wireless Commun.*, vol. 19, no. 4, pp. 2411–2426, Apr. 2020.

[8] I. Mademlis et al., "High-level multiple-UAV cinematography tools for covering outdoor events," *IEEE Trans. Broadcast.*, vol. 65, no. 3, pp. 627–635, Sep. 2019.

[9] L. Zhong, M. Wang, C. Xu, S. Yang, and G.-M. Muntean, "Decentralized optimization for multicast adaptive video streaming in edge cache-assisted networks," *IEEE Trans. Broadcast.*, vol. 69, no. 3, pp. 812–822, Sep. 2023, doi: 10.1109/TBC.2023.3254165.

[10] H. Zhu, Y. Cao, T. Jiang, and Q. Zhang, "Scalable NOMA multicast for SVC streams in cellular networks," *IEEE Trans. Commun.*, vol. 66, no. 12, pp. 6339–6352, Dec. 2018.

[11] M. N. Dani, D. K. So, J. Tang, and Z. Ding, "Resource allocation for layered multicast video streaming in NOMA systems," *IEEE Trans. Veh. Technol.*, vol. 71, no. 11, pp. 11379–11394, Nov. 2022.

[12] E. Lakiotakis, P. Sermpezis, and X. Dimitropoulos, "Joint optimization of UAV placement and caching under battery constraints in UAV-aided small-cell networks," in *Proc. ACM SIGCOMM Workshop Mobile AirGround Edge Comput. Syst. Netw. Appl.*, 2019, pp. 8–14.

[13] T. Zhang, Z. Wang, Y. Liu, W. Xu, and A. Nallanathan, "Caching placement and resource allocation for cache-enabling UAV NOMA networks," *IEEE Trans. Veh. Technol.*, vol. 69, no. 11, pp. 12897–12911, Nov. 2020.

[14] S. Chai and V. K. Lau, "Mixed-timescale request-driven user association, trajectory and radio resource control for cache-enabled multi-UAV networks," *IEEE Trans. Signal Process.*, vol. 70, pp. 4997–5011, 2022.

[15] B. Zeng, C. Zhan, Y. Yang, and J. Liao, "Access delay minimization for scalable videos in cache-enabled multi-UAV networks," in *Proc. IEEE Glob. Commun. Conf.*, 2022, pp. 389–394.

[16] X. Guo, C. Zhang, F. Yu, and H. Chen, "Coverage analysis for UAV-assisted mmWave cellular networks using poisson hole process," *IEEE Trans. Veh. Technol.*, vol. 71, no. 3, pp. 3171–3186, Mar. 2022.

[17] N. Chukhno, O. Chukhno, S. Pizzi, A. Molinaro, A. Iera, and G. Araniti, "Efficient management of multicast traffic in directional mmWave networks," *IEEE Trans. Broadcast.*, vol. 67, no. 3, pp. 593–605, Sep. 2021.

[18] B. Li, X. Guo, J. Cong, and R. Zhang, "Sliding-window-based RNC scheme in UAV Multicasting: Performance analysis and network optimization," *IEEE Internet Things J.*, vol. 9, no. 14, pp. 12111–12124, Jul. 2022.

[19] I.-S. Comşa, G.-M. Muntean, and R. Trestian, "An innovative machine-learning-based scheduling solution for improving live UHD video streaming quality in highly dynamic network environments," *IEEE Trans. Broadcast.*, vol. 67, no. 1, pp. 212–224, Mar. 2021.

[20] W. Miao, C. Luo, G. Min, and Z. Zhao, "Lightweight 3-D beamforming design in 5G UAV broadcasting communications," *IEEE Trans. Broadcast.*, vol. 66, no. 2, pp. 515–524, Jun. 2020.

[21] M. Ghermezcheshmeh, V. Shah-Mansouri, and M. Ghanbari, "Analysis and performance evaluation of scalable video coding over heterogeneous cellular networks," *Comput. Netw.*, vol. 148, pp. 151–163, Jan. 2019.

[22] M. Katwe, K. Singh, P. K. Sharma, C.-P. Li, and Z. Ding, "Dynamic user clustering and optimal power allocation in UAV-assisted full-duplex hybrid NOMA system," *IEEE Trans. Wireless Commun.*, vol. 21, no. 4, pp. 2573–2590, Apr. 2022.

[23] F. Qi, L. Liu, W. Xie, and Z. Sun, "Fountain coded coordinated multipoint for 5G MBMS UAV relay," *IEEE Trans. Broadcast.*, early access, Jul. 21, 2023, doi: 10.1109/TBC.2023.3291141.

[24] H. Zeng, X. Zhu, Y. Jiang, and Z. Wei, "UAV-ground BS coordinated NOMA with joint user scheduling, power allocation and trajectory design," in *Proc. IEEE Int. Conf. Commun.*, 2020, pp. 1–6.

[25] S. Salar Hosseini, M. R. Javan, and A. Nazari, "Multicasting in NOMA-based UAV networks: Path design and throughput maximisation," *IET Commun.*, vol. 16, no. 14, pp. 1708–1723, 2022.

[26] L. Wang, H. Zhang, S. Guo, and D. Yuan, "Deployment and association of multiple UAVs in UAV-assisted cellular networks with the knowledge of statistical user position," *IEEE Trans. Wireless Commun.*, vol. 21, no. 8, pp. 6553–6567, Aug. 2022.

[27] Y. Li, S. Xu, Y. Wu, and D. Li, "Network energy-efficiency maximization in UAV-enabled air–ground-integrated deployment," *IEEE Internet Things J.*, vol. 9, no. 15, pp. 13209–13222, Aug. 2022.

[28] A. Al-Hourani, S. Kandeepan, and S. Lardner, "Optimal LAP altitude for maximum coverage," *IEEE Wireless Commun. Lett.*, vol. 3, no. 6, pp. 569–572, Dec. 2014.

[29] H. Zhao, H. Wang, W. Wu, and J. Wei, "Deployment algorithms for UAV airborne networks toward on-demand coverage," *IEEE J. Sel. Areas Commun.*, vol. 36, no. 9, pp. 2015–2031, Sep. 2018.

[30] C. A. Balanis, *Antenna Theory: Analysis and Design*. Hoboken, NJ, USA: Wiley, 2016.

[31] H. He, S. Zhang, Y. Zeng, and R. Zhang, "Joint altitude and beamwidth optimization for UAV-enabled multiuser communications," *IEEE Commun. Lett.*, vol. 22, no. 2, pp. 344–347, Feb. 2018.

[32] Q. Ye, W. Zhuang, S. Zhang, A.-L. Jin, X. Shen, and X. Li, "Dynamic radio resource slicing for a two-tier heterogeneous wireless network," *IEEE Trans. Veh. Technol.*, vol. 67, no. 10, pp. 9896–9910, Oct. 2018.

[33] H. Shen, Q. Ye, W. Zhuang, W. Shi, G. Bai, and G. Yang, "Drone-small-cell-assisted resource slicing for 5G uplink radio access networks," *IEEE Trans. Veh. Technol.*, vol. 70, no. 7, pp. 7071–7086, Jul. 2021.

[34] D. Comaniciu and P. Meer, "Mean shift analysis and applications," in *Proc. IEEE Int. Conf. Comput. Vis.*, vol. 2, 1999, pp. 1197–1203.

[35] P. R. Östergård, "A fast algorithm for the maximum clique problem," *Discret. Appl. Math.*, vol. 120, nos. 1–3, pp. 197–207, 2002.

[36] J. Wu, C.-M. Li, L. Jiang, J. Zhou, and M. Yin, "Local search for diversified top-k clique search problem," *Comput. Oper. Res.*, vol. 116, Apr. 2020, Art. no. 104867.

[37] I.-P. Belikaidis, A. Georgakopoulos, E. Kosmatos, V. Frascolla, and P. Demestichas, "Management of 3.5-GHz spectrum in 5G dense networks: A hierarchical radio resource management scheme," *IEEE Veh. Technol. Mag.*, vol. 13, no. 2, pp. 57–64, Jun. 2018.

[38] J. Lee, B. C. Yeo, J.-S. Kim, M. S. Jang, and J. K. Choi, "Energy efficient scalable video coding based cooperative multicast scheme with selective layer forwarding," *IEEE Commun. Lett.*, vol. 17, no. 6, pp. 1116–1119, Jun. 2013.

[39] Z. Tong, H. Shen, N. Shi, T. Wang, and G. Bai, "Joint resource optimization for nonorthogonal multiple access-enhanced scalable video coding multicast in unmanned aerial vehicle-assisted radio-access networks," *ETRI J.*, vol. 45, no. 5, pp. 874–886, 2023, doi: 10.4218/etrij.2022-0136.

[40] T. M. Nguyen, W. Ajib, and C. Assi, "A novel cooperative NOMA for designing UAV-assisted wireless backhaul networks," *IEEE J. Sel. Areas Commun.*, vol. 36, no. 11, pp. 2497–2507, Nov. 2018.

[41] D. Zhai, H. Li, X. Tang, R. Zhang, Z. Ding, and F. R. Yu, "Height optimization and resource allocation for NOMA enhanced UAV-aided relay networks," *IEEE Trans. Commun.*, vol. 69, no. 2, pp. 962–975, Feb. 2021.

Ziyuan Tong received the B.S. degree in computer science from the Nanjing University Jinling College, Nanjing, China, and the M.S. degree (with Hons.) in computer science from Nanjing Tech University, Nanjing. Her research interests include space-air-ground integrated networks, non-orthogonal multiple access, resource management, and layer-aware wireless video multicasting.

Tianjing Wang (Member, IEEE) received the B.Sc. degree in mathematics from Nanjing Normal University in 2000, the M.Sc. degree in mathematics from Nanjing University in 2002, and the Ph.D. degree in signal and information system from the Nanjing University of Posts and Telecommunications in 2009, where she was a Full-Time Postdoctoral Fellow with the School of Electronic Science and Engineering from 2011 to 2013. From 2013 to 2014, she was a Visiting Scholar with the ECE Department, State University of New York at Stony Brook. She is an Associate Professor with the Department of Communication Engineering, Nanjing Tech University. Her research interests include distributed machine learning for multimedia networking and cellular V2X communication networks.

Hang Shen (Member, IEEE) received the Ph.D. degree (with Hons.) in computer science from the Nanjing University of Science and Technology. He worked as a Full-Time Postdoctoral Fellow with the Broadband Communications Research Lab, ECE Department, University of Waterloo, Waterloo, ON, Canada, from 2018 to 2019. He is an Associate Professor with the Department of Computer Science and Technology, Nanjing Tech University, Nanjing, China. He has published research papers in international journals and conferences, including the IEEE TRANSACTIONS ON MOBILE COMPUTING, IEEE TRANSACTIONS ON VEHICULAR TECHNOLOGY, *Journal of Systems Architecture*, and IEEE ICC. His research interests involve space-air-ground integrated networks, multimedia networking, network security, and blockchain. He is an Associate Editor of the IEEE ACCESS and an Academic Editor of the *Mathematical Problems in Engineering*. He was a Guest Editor of the *Peer-to-Peer Networking and Applications* and a TPC Member of the Annual International Conference on Privacy, Security and Trust in 2021.

Guangwei Bai received the B.Eng. and M.Eng. degrees in computer engineering from Xi'an Jiaotong University, Xi'an, China, in 1983 and 1986, respectively, and the Ph.D. degree in computer science from the University of Hamburg, Hamburg, Germany, in 1999. From 1999 to 2001, he worked as a Research Scientist with the German National Research Center for Information Technology, Germany. In 2001, he joined the University of Calgary, Calgary, AB, Canada, as a Research Associate. Since 2005, he has been working with Nanjing Tech University, Nanjing, China, as a Professor of Computer Science. From October to December 2010, he was a Visiting Professor with the ECE Department, University of Waterloo, Waterloo, ON, Canada. He has authored and coauthored more than 70 peer review papers in international journals and conferences including IEEE TRANSACTIONS ON MOBILE COMPUTING, IEEE TRANSACTIONS ON VEHICULAR TECHNOLOGY, *Performance Evaluation*, *Ad Hoc Networks*, *Journal of Systems Architecture*, IEEE ICC, and IEEE LCN. His research interests include architecture and protocol design for future networks, multimedia networking, cybersecurity, and privacy computing. He is a member of ACM and a Distinguished Member of CCF.